# Dynamic Performance of DC-DC-AC Boost Switched Capacitor Converter Fed Single Phase Induction Motor

Crescent Onyebuchi Omeje

Department of Electrical/Electronic Engineering, Faculty of Engineering, University of Port Harcourt, Choba, Port-Harcourt, Rivers State, Nigeria
crescent.omeje@uniport.edu.ng

*Abstract*: Single phase induction motor mostly exhibits a low starting torque and also produces a significant level of torque pulsations during a steady state acceleration time. These drawbacks can be mitigated using an improved drive strategy. The drive scheme applied in this work employed a DC-DC-AC boost switched capacitor converter to drive a 0.25 horse power single phase induction motor at a regulated duty cycle of 0.5 and 0.75. The motor was simulated under steady state and transient state at a varying load torque of 0-22.5Nm. The converter topology integrates the inductive switching cell with a switched capacitor in performing a direct energy conversion at a high output voltage gain. A simulation process carried out on the complete drive model showed that an enhanced starting torque and a speed regulation values of 0.2255 and 0.9271 were obtained at 0.5 and 0.75 duty cycle under steady state whereas 0.2094 and 0.2096 were obtained under transient state. The results obtained also showed that different efficiency values of 82.86% and 76.79% were achieved at 0.75 and 0.5 duty cycle. A stable motor operation with an improved voltage gain, appreciable power output and reduced torque pulsations were achieved at 0.75 duty cycle. All simulation processes were accomplished in MATLAB/SIMULINK 2014.

*Keywords*: DC-DC-AC Boost Converter, Duty-Cycle, Single-Phase Inverter, Single-Phase Induction Motor, Speed and Torque control, Voltage-gain.

## 1. Introduction

Switched capacitor converters (SCC) are mostly applied in single phase low-voltage electronic circuit due to the obvious simplicity and high rate of energy conversion process [1]. The first circuit topology involving SCC was applied in voltage doublers circuit and presented in [2-3]. Other topologies that are aimed at improving the efficiency of the electrical device at higher voltage gains are also presented in [4-5]. Pure ac-ac switched capacitor converters have been developed for three phase systems with good performance and proven portability as reported in [6-8]. The hybrid boost switched capacitor converter has been deployed in dc-dc converter systems and referenced in [9-12]. However, the use of switched capacitor converter (SCC) in ac-ac conversion system has not previously gained wide range of applications due to inherent switching losses and unwarranted communication stages. The DC-DC-AC boost switched capacitor converter applied in this paper provides a high voltage gain, an appreciable output power and an output voltage which is approximately five times the value of the input voltage. The main objective of this paper is to derive an optimal supply voltage that can drive a single phase induction motor with a good speed regulation, reduced losses and an enhanced efficiency. The circuit topology is presented in Figure 1. It is a combination of a boost converter with a switched capacitor connected single phase inverter powered load which can either be a resistive load or an induction motor.

Received: April 13rd, 2022. Accepted: June 25th, 2022
DOI: 10.15676/ijeei.2022.14.2.13

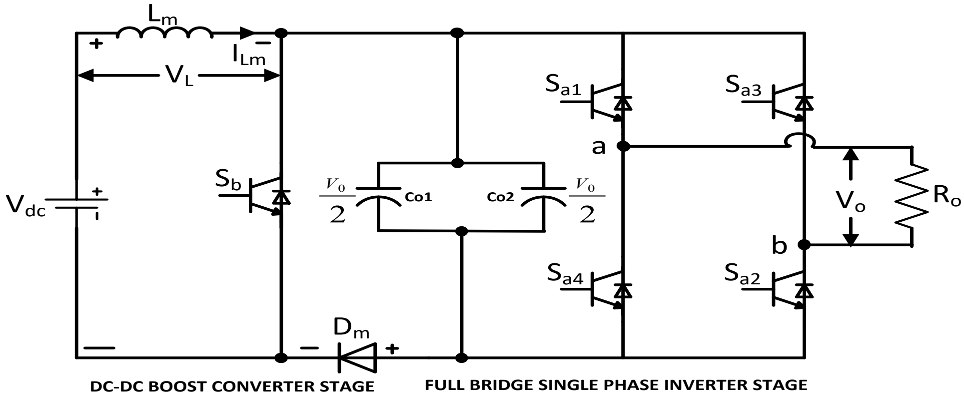


Figure 1. DC-DC-AC Boost Switched Capacitor Converter.

## 2. DC-DC-AC Converter Circuit Operation

The circuit operation is composed of two stages. Stage 1: input dc source which is connected in series to an inductor, a MOSFET switch and an output capacitor. This stage forms the dc boost converter stage. The boost converter converts an unregulated d.c voltage input $V_{dc}$ into a variable dc output voltage $V_o$ such that $V_{dc} \leq V_o$ as referenced in [13], and buttressed in equation (1).

$$\frac{V_o}{V_{dc}} = \frac{1}{1-D} \tag{1}$$

The output voltage therefore is been regulated by the converters duty cycle and for the scope of this paper, the duty cycle (D) was kept at 0.5 and 0.75 to test for optimum performance.
Stage 2: this is the inverter stage which consists of the output dc capacitor boosted voltage, four IGBT switches and the load output which can take the form of a resistive load or simply an induction motor. The four IGBT switches that make up the inverter stage are complementarily turned on in conformity with the sequence presented in Figure 2. $S_{a1}$ is complementary to $S_{a4}$ while $S_{a2}$ is complementary to $S_{a3}$

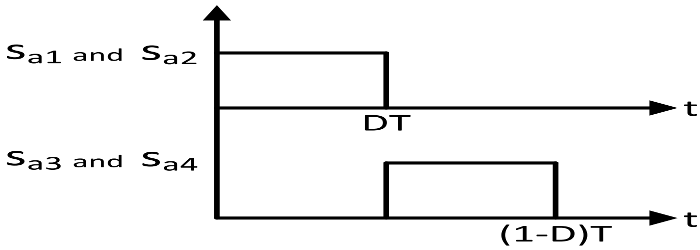


Figure 2. Single Phase Inverter Switching Sequence.

When the capacitances in Figure 1 are large enough, the voltages across the capacitors are considered constant during the period of operation. Therefore, the average voltage values are equal and are given by equation (2).

$$V_{co1} = V_{co2} = \frac{V_o}{2} \tag{2}$$

Considering the positive half cycle (first operating stage) and negative half cycle (second operating stage), the average voltage across the inductor $L_m$ is given by equation (3).

$$V_L = L_m \frac{di_{Lm}}{dt} = V_{dc} - (1-D) \times \frac{V_o}{2} \tag{3}$$

During the inverter switching period, equation (3) changes to (4) with the transient and steady states present.

$$V_L = \begin{cases} L_m \frac{di_{Lm}}{dt} \\ \textit{Transient state} \end{cases} + \begin{cases} j\omega L i_{Lm} \\ \textit{Steady State} \end{cases} \quad (4)$$

Substituting equation (4) into equation (3) with the derivative of average inductor current equal to zero $\frac{di_{Lm}}{dt} = 0$ gives rise to the converter's output voltage as a function of duty cycle and inductance as shown in equation (5).

$$V_o = \frac{2}{1-D}[V_{in} - j\omega L_m i_{Lm}] \quad (5)$$

Similarly, the inductor current equation in terms of capacitors and converter duty cycle is given by equation (6).

$$i_{Lm} = \frac{2}{1-D} i_o + \frac{j\omega(C_{o1}+C_{o2})}{2(1-D)} V_o \quad (6)$$

Substituting equation (6) into equation (5) gives rise to equations (7a) and (7b)

$$V_o = \frac{2}{1-D}\left(V_{in} - j\omega L_m\left(\frac{2}{1-D} i_o + \frac{j\omega(C_{o1}+C_{o2})}{2(1-D)} V_o\right)\right) \quad (7a)$$

$$V_o = \left(\frac{2}{1-D} V_{in} - j\frac{4\omega L_m}{(1-D)^2} i_o + \frac{\omega^2 L_m(C_{o1}+C_{o2})}{(1-D)^2} V_o\right) \quad (7b)$$

Since $i_o = \frac{V_o}{Z_o} = \frac{V_o}{R_o + jX_o} = \frac{V_o(R_o - jX_o)}{R_o{}^2 + X_o{}^2} = \frac{V_o(R_o - jX_o)}{z_o^2}$. Simplifying equation (7b) in terms of voltage gain gives rise to equations (8a) and (8b)

$$V_o\left(1 - \frac{\omega^2 L_m(C_{o1} + C_{o2})}{(1-D)^2}\right) = \frac{2}{1-D} V_{in} - j\frac{4\omega L_m}{(1-D)^2} \times \frac{V_o(R_o - jX_o)}{z_o^2} \quad (8a)$$

$$V_o\left(1 - \frac{\omega^2 L_m(C_{o1} + C_{o2})}{(1-D)^2} + \frac{4\omega L_m X_o}{z_o^2(1-D)^2} + j\frac{4\omega L_m R_o}{z_o^2(1-D)^2}\right) = \frac{2}{1-D} V_{in} \quad (8b)$$

The converters voltage gain as a function of duty cycle and inductance is given by equation (9).

$$\frac{V_o}{V_{in}} = \frac{\frac{2}{1-D}}{1 - \frac{\omega^2 L_m(C_{o1}+C_{o2})}{(1-D)^2} + \frac{4\omega L_m X_o}{z_o^2(1-D)^2} + j\frac{4\omega L_m R_o}{z_o^2(1-D)^2}} \quad (9)$$

The magnitude and phasor of voltage gain at varied duty cycle and different inductances are obtained from equations (10a) and (10b).

$$\left|\frac{V_o}{V_{in}}\right| = \left|\frac{2z_o^2(1-D)}{z_o^2(1-D)^2 - \omega^2 z_o^2 L_m(C_{o1} + C_{o2}) + 4\omega L_m X_o} - \frac{j2z_o^2(1-D)}{4\omega L_m R_o}\right| \quad (10a)$$

$$\theta = \tan^{-1}(|A - jB|) \quad (10b)$$

Where $A = \frac{2z_o^2(1-D)}{z_o^2(1-D)^2 - \omega^2 z_o^2 L_m(C_{o1} + C_{o2}) + 4\omega L_m X_o}$ and $B = \frac{2z_o^2(1-D)}{4\omega L_m R_o}$

In Figure 3, it can be observed that the converter's output voltage increases as the duty cycle value increases and follows the same pattern of increase that is in agreement with equation (5). Therefore, for a safe operation of the converter within a permissible voltage limit, a duty cycle range of 0.5-0.75 was adopted by extrapolation while inductance values within the range of 3.966mH and 4.25mH were chosen. Above 0.75 duty cycle and 4.25mH inductance, an over voltage region is attained which may be lethal to the converter's operation and may also result in reverse motor operation.

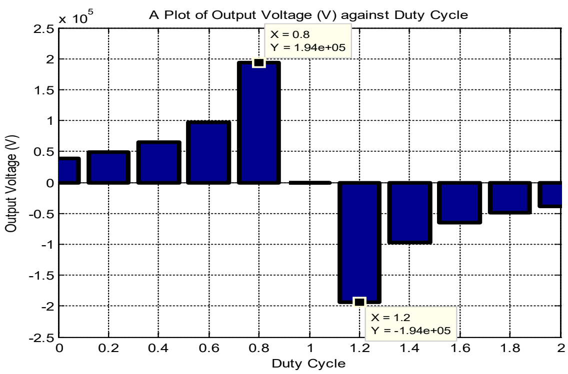


Figure 3. Converter Output Voltage against Duty Cycle

## 3. Methodology: Modeling of Single Phase Capacitor Start and Capacitor Run Induction Motor.

Single phase induction motors are classified based on their mode of starting and are also referred to by the names descriptive of these modes. Exact selection of the right motor is entirely based on the starting and running torque requirement of the load, the duty cycle of the driven load and the limitations on the starting and running current from the supply [14]. Generally, single phase induction motors (SPIMs) are small motors mostly built in fractional horse power range of ¼ HP and applied in low power devices [15]. Its starting mechanism requires special arrangement such as an auxilliary winding provided at the stator since the motor operates on one stator winding [16]. The SPIMs are reliable, robust, cheap and are used in homes and offices for air conditioners, refrigerators, washing machines, furnace fans and garbage disposal. Its major disadvantages are not limited to low power factor, high starting current, and sometimes low efficiency which gives rise to great energy wastage [17]. It is inhereently non-self starting and cannot accommodate heavy loads [18]. The capacitor start and capacitor run induction motor (CSCRIM) has two capacitors connected in parallel. The smaller capacitor $C_{run}$ required for optimum running condition is permanently connected with the auxilliary winding while the larger capacitor $C_{start}$ is connected with the $C_{run}$ for efficient starting as shown in Figure 4. The motor combines the advantages of capacitor-run and capacitor-start motors with a good running power factor, improved efficiency, smooth running operation and improved starting torque [19]. The starting capacitor $C_{start}$ is always disconnected when the motor speed approaches 75% of the synchronous speed value and at this state the motor runs as a single phase induction motor [20].

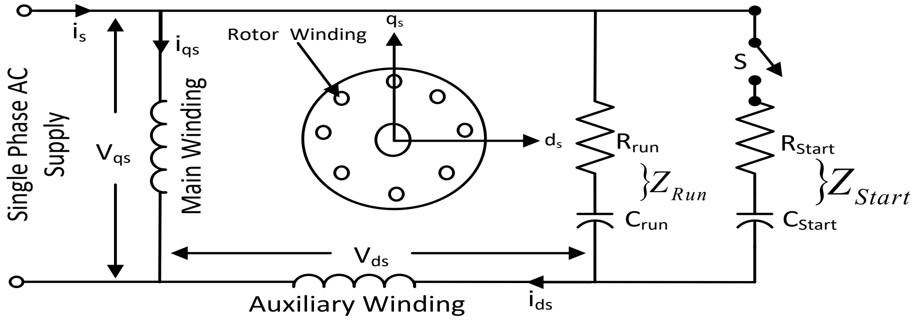


Figure 4. Circuit Diagram of Capacitor Start Capacitor Run Single Phase Induction Motor.

The dq modelling of capacitor start capacitor run induction motor is achieved with the aid of the equivalent circuit diagram presented in Figure 4. At start, the switch S is turned on thereby connecting the capacitor-start with the auxilliary winding (Starting winding). Since Vqs = Vs, the voltage across the auxilliary winding during starting is given by equation (11).

$$V_{ds} = V_s - \frac{1}{Z_{eq}} \int i_{ds}\, dt \qquad (11)$$

Where $Z_{eq} = Z_{run} \parallel Z_{start} = (R_{run} + jXc_{run}) \parallel (R_{start} + jXc_{start}) = \frac{(R_{run} + jXc_{run}) \times (R_{start} + jXc_{start})}{(R_{run} + jXc_{run}) + (R_{start} + jXc_{start})}$

When the motor speed attains 75% of the synchronous speed value the switch S is turned off with the capacitor-start disconnected from the auxilliary winding. During this running operation at 75% synchronous speed, the voltage across the auxilliary winding is then given by equation (12).

$$V_{ds} = V_s - \frac{1}{Z_{run}} \int i_{ds}\, dt \qquad (12)$$

The general dq voltage equations of a single phase induction motor in accordance with Chee Mu Ong, Krause et al [21-27] are given by equations (13) - (16).

$$V_{qs} = R_{qs}\, i_{qs} + \frac{d\lambda_{qs}}{dt} \quad (V) \qquad (13)$$

$$V_{ds} = R_{ds}\, i_{ds} + \frac{d\lambda_{ds}}{dt} \quad (V) \qquad (14)$$

$$V'^{s}_{qr} = R'_r i'^{s}_{qr} - \omega_r \lambda'^{s}_{dr} + \frac{d\lambda'^{s}_{qr}}{dt} \quad (V) \qquad (15)$$

$$V'^{s}_{dr} = R'_{r} i'^{s}_{dr} + \omega_r \lambda'^{s}_{qr} + \frac{d\lambda'^{s}_{dr}}{dt} \quad (V) \tag{16}$$

The flux linkage equations presented in equations (17) – (20).

$$\lambda_{qs} = L_{Lqs} i_{qs} + L_{mq}\left(i_{qs} + i'^{s}_{qr}\right) \tag{17}$$

$$\lambda_{ds} = L_{Lds} i_{ds} + L_{mq}\left(i_{ds} + i'^{s}_{dr}\right) \tag{18}$$

$$\lambda'_{qr} = L'_{Lqr} i'_{qr} + L_{mq}\left(i_{qs} + i'^{s}_{qr}\right) \tag{19}$$

$$\lambda'_{dr} = L'_{Ldr} i'_{dr} + L_{mq}\left(i_{ds} + i'^{s}_{dr}\right) \tag{20}$$

For accuracy in simulation, equations (17) to (20) are rearranged in terms of electrical base angular velocity and represented in equations (21) to (24). Where $\psi = \omega_b \lambda$

$$\psi^{s}_{qs} = \omega_b \int \left\{ V^{s}_{qs} + \frac{r_{qs}}{X_{Lqs}}\left(\psi_{mq} - \psi^{s}_{qs}\right) \right\} dt \tag{21}$$

$$\psi^{s}_{ds} = \omega_b \int \left\{ V^{s}_{ds} + \frac{r_{ds}}{X_{Lds}}\left(\psi_{md} - \psi'^{s}_{ds}\right) \right\} dt \tag{22}$$

$$\psi'^{s}_{qr} = \omega_b \int \left\{ V^{is}_{qr} + \frac{\omega_r}{\omega_b}\psi'^{s}_{dr} + \frac{r'_r}{X'_{Lqr}}\left(\psi_{mq} - \psi'^{s}_{qr}\right) \right\} dt \tag{23}$$

$$\psi'^{s}_{dr} = \omega_b \int \left\{ V'^{s}_{dr} - \frac{\omega_r}{\omega_b}\psi'^{s}_{qr} + \frac{r'_r}{X'_{Ldr}}\left(\psi_{md} - \psi'^{s}_{dr}\right) \right\} dt \tag{24}$$

$$\psi_{mq} = X_{mq}\left(i_{qs} + i'^{s}_{qr}\right) \tag{25}$$

$$\psi_{md} = X_{mq}\left(i'_{ds} + i'^{s}_{dr}\right) \tag{26}$$

$$i_{qs} = \frac{\psi_{qs} - \psi_{mq}}{X_{Lqs}} \tag{27}$$

$$i_{ds} = \frac{\psi_{ds} - \psi_{md}}{X'_{Ldr}} \tag{28}$$

$$i'^{s}_{qr} = \frac{\psi'^{s}_{qr} - \psi_{mq}}{X'_{Lqr}} \tag{29}$$

$$i'^{s}_{dr} = \frac{\psi'^{s}_{dr} - \psi_{md}}{X'_{Ldr}} \tag{30}$$

Substituting equations (27)-(30) into equations (25) and (26) gives rise to equations (31) and (32).

$$\psi_{mq} = X_{Mq}\left(\frac{\psi_{qs}}{X_{Lqs}} + \frac{\psi'^{s}_{qr}}{X'_{Lqr}}\right) \tag{31}$$

$$\psi_{md} = X_{Md}\left(\frac{\psi_{ds}}{X_{Lds}} + \frac{\psi'^{s}_{dr}}{X'_{Ldr}}\right) \tag{32}$$

$$\frac{1}{X_{Mq}} = \frac{1}{X_{mq}} + \frac{1}{X_{Lqs}} + \frac{1}{X'_{Lr}} \tag{33}$$

$$\frac{1}{X_{Md}} = \frac{1}{X_{md}} + \frac{1}{X_{Lds}} + \frac{1}{X'_{Lr}} \tag{34}$$

The mechanical model equation of motional torque and speed for the rotor axis is obtained by equating the inertia torque to the accelerating torque as depicted in (35).

$$J\frac{d\omega_m}{dt} = T_{em} - T_{mech} - T_{damp} \quad (N.m) \tag{35}$$

$T_{mech}$ is the externally applied mechanical load torque and $T_{damp}$ is the damping torque which is in the direction opposite to the rotation of the rotor and its equation is presented in (36).

$$T_{damp} = B\omega_m \quad (N.m) \tag{36}$$

Where: B = coefficient of viscosity or damping coefficient (N.M.S) and $\omega_m$ = mechanical speed in Rad/Sec. An open loop control block diagram that summarizes the operation of the power electronics and machine modelling is presented in Figure 5 while the complete circuit model for the DC-DC-AC switched capacitor converter fed induction motor is as well presented in Figure 6. The Simulink model is shown in Appendix 1.

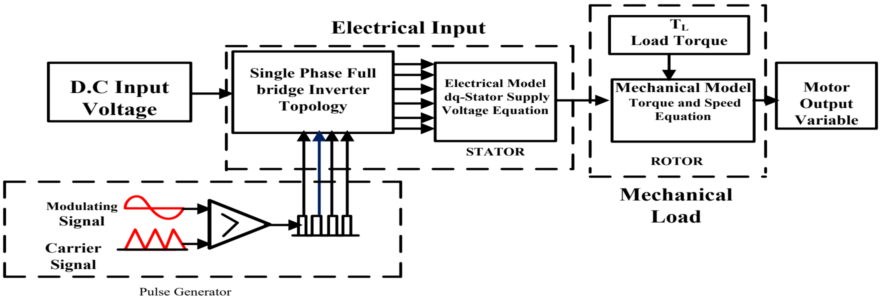


Figure 5. An Open loop Block Diagram of Single-Phase DC-AC switched capacitor converter fed Induction Machine.

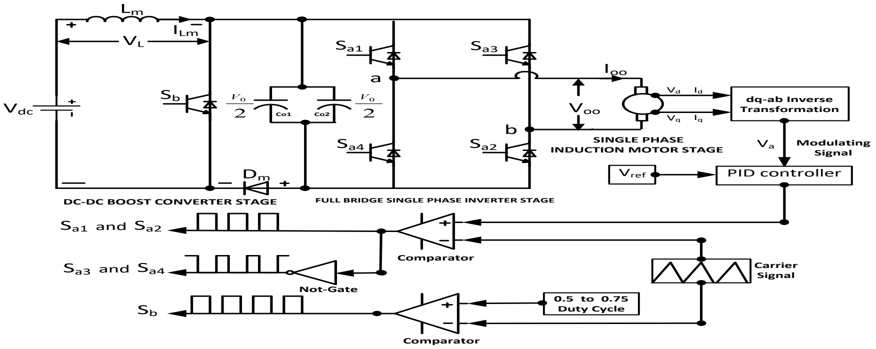


Figure 6. A Controlled Circuit Diagram of the Single-Phase DC-DC-AC switched capacitor converter fed Induction Machine.

Table 1. Motor and Converter Simulation Parameter

| PARAMETERS | VALUES |
|---|---|
| DC-DC Converter Rated Input Voltage (Volts) | 220 |
| Inductance Values (mH) | 6, 8, 10 |
| Output capacitor Values $C_{o1}$ and $C_{o2}$ (μF) | 220 |
| Converter output Resistance (Ω) | 50 |
| Converter duty cycle | 0.5 and 0.75 |
| Induction Motor Rated Power (H.P) | 0.25 |
| Main Winding Stator Resistance (Ω) | 2.02 |
| Auxiliary Winding Stator Resistance (Ω) | 4.12 |
| Main Winding Stator Leakage Inductance $L'_{Ls}$ (mH) | 7.4 |
| Auxiliary Winding Leakage Inductance $L'_{Lr}$ ( mH) | 5.6 |
| Main Winding Mutual Inductance ( mH) | 177.2 |
| Number of Pole Pair | 2 |
| Frequency (Hertz) | 50 |
| Motor Speed (RPM) | 1440 |
| Coefficient of Viscosity (Nms) | 0.0008 |
| Motor Inertia (Kg-M$^2$) | 0.016 |
| Load Torque (Nm) | 7.5 |
| Capacitor Start Value (μF) | 2 |

**4. Simulation Results and Discussions**

The switching pulses for the single phase inverter is shown in Figure 7. Switches $S_{a1}$ and $S_{a2}$ are turned on by the same signal and are also complementary to switches $S_{a3}$ and $S_{a4}$. The DC-DC converter input voltage waveform is presented in Figure 8 which conforms with the numerical value presented in Table 1. The steady state simulaton results are presented in Figures 9-18 while the results obtained during transient states are shown in Figures 19-43. The converter inductor current at 0.5 and 0.75 duty cycles operation are presented in Figures 9 and 10. A surge in inductor current value was observed at start which peaks at 165.5A at 0.5 duty cycle and 485.5A at 0.75 duty cycle due to high slip value and low rotor resistance during starting. The steady state settling time of 0.199 Sec. was attained at 0.75 duty cycle as opposed to 0.4832 Sec. obtained at 0.5 duty cycle operation. In Figures 11 and 12, the power input value of 61.98 KW was obtained at 0.2069 Sec for 0.75 duty cycle in contrast to the 18.8 KW obtained at 0.448 Sec for 0.5 duty cycle. In Figures 13 and 14, an improved power output of 70.05 KW at 0.2065 Sec was achieved at 0.75 duty cycle while 18.17KW at 0.6472 Sec was obtained at 0.5 duty cycle. Similarly, Figures 15 and 16 showed that the steady state settling time of 0.3356 Sec was attained by the motor speed at 0.75 duty cycle at a faster rate than the 0.6058 Sec achieved with 0.5 duty cycle. Figures 17 and 18 also showed that torque pulsations are more pronounced at 0.5 duty cycle. The transient state inductor current of the DC to DC converter presented in Figure 19 at 0.75 duty cycle showed that at a simulation time of [0.4072 to 0.8037]Sec and [1.404 to 1.809]Sec, the inductor current values changed from 288.9A to 311.6A and from 287.3A to 313.2A. These abrupt changes corresponded with the systemic loading at 0.75 duty cycle.

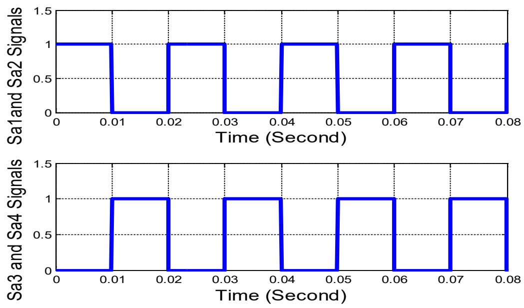


Figure 7. Switching pulses of Single Phase Inverter

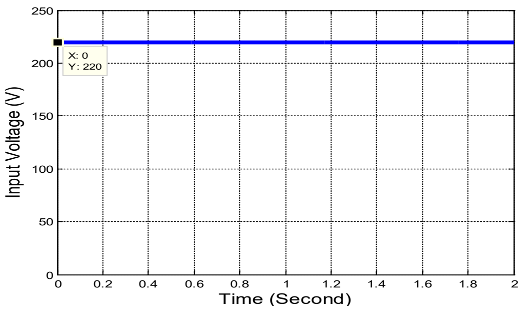


Figure 8. DC Input Voltage of Single Phase Inverter

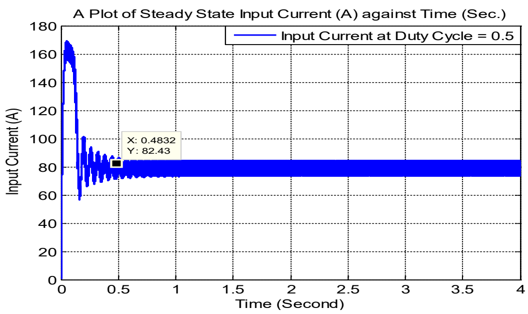


Figure 9. Converter Inductor Current of at D = 0.5

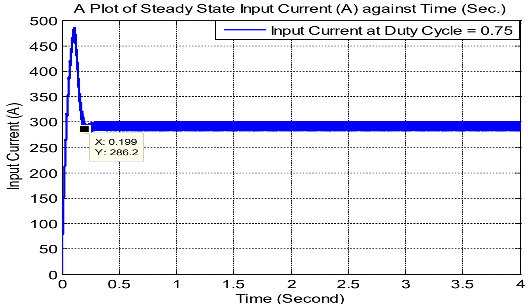


Figure 10. Converter Inductor Current of at D = 0.75.

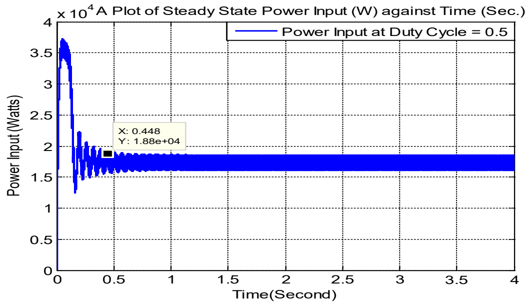


Figure 11. DC-DC Converter Power Input at D = 0.5

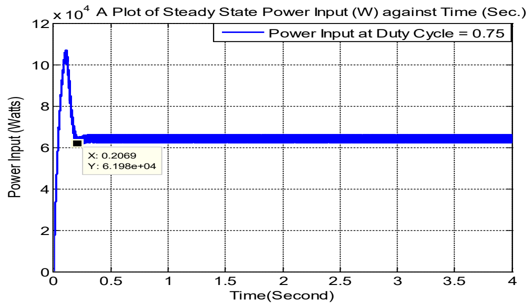


Figure 12. DC-DC Converter Power Input at D = 0.75.

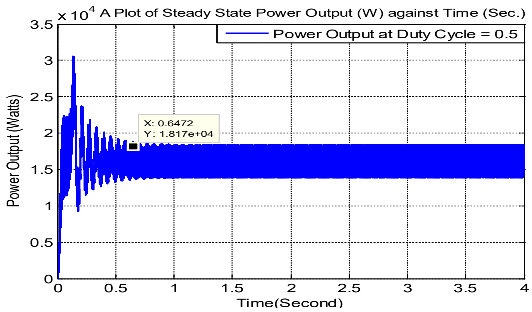


Figure 13. DC-DC Converter Power output at D = 0.5

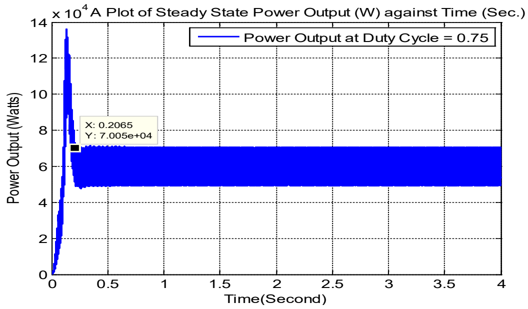


Figure 14. DC-DC Converter Power output at D = 0.75.

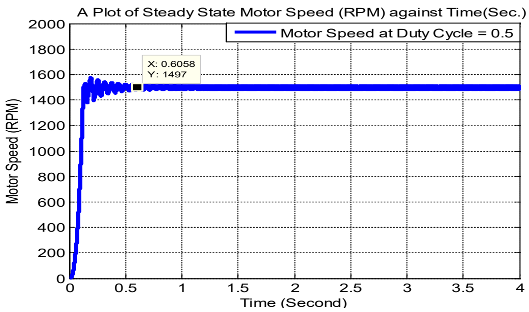


Figure 15. Motor Speed at D = 0.5 and on no-load

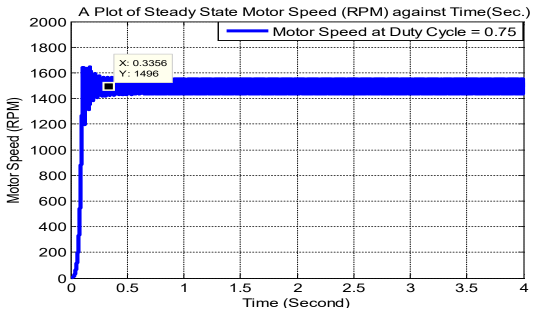


Figure 16. Motor Speed at D = 0.75 and on no-load.

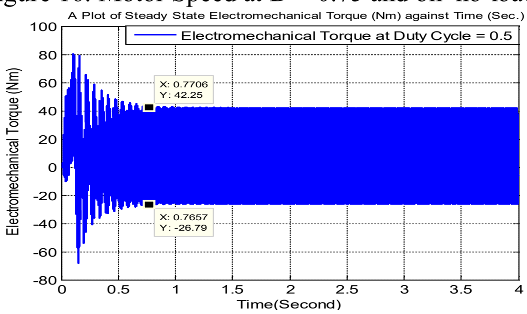


Figure 17. Motor Torque at D = 0.5 and on no-load

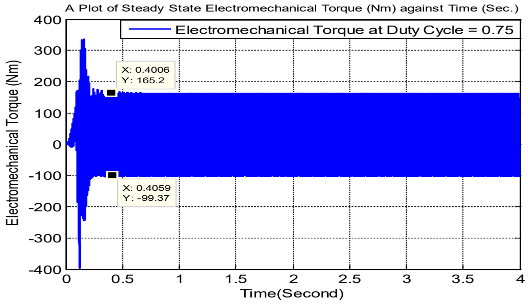


Figure 18. Motor Torque at D = 0.75 and on no-load.

The simulation waveforms for the transient state dynamic performance are shown in Figures 19-43 respectively.

The peak value of the inductor current of 483.1A at a rise time of 0.1083Sec is evident of its affinity for current at start. In Figure 20, a sharp rise was observed in the value of the input power of 105.9 KW at 0.101Sec which reduced to 65.1 KW and 69.31 KW at 0.403Sec and 0.8035Sec during machine loading. In Figure 21, a high value of switched capacitor output voltage was obtained which is almost 4.45 multiple of the input voltage. This high value is indicative of high boosting capacity of the converter at 0.75 duty cycle. The waveforms for the output current and power output of the DC-DC boost converter are presented in Figures 22 and 23. At start, the power output peaks at 136.3 KW at 0.1366Sec. This peak value decreased correspondingly as the load is applied within the period of [0.411 to 0.8166]Sec. and [1.421 to 1827]Sec. The efficiency of the converter obtained as 82.86% at 0.75 duty cycle was calculated based on the simulation values derived from Figures 20 and 23.

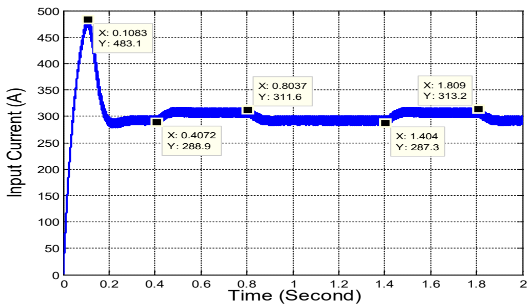


Figure 19. Inductor Current of DC-DC Boost Converter

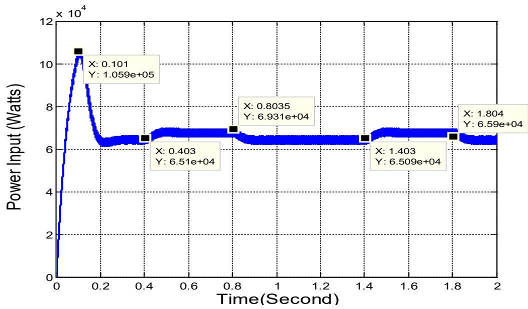


Figure 20. Input Power of the DC-DC Converter.

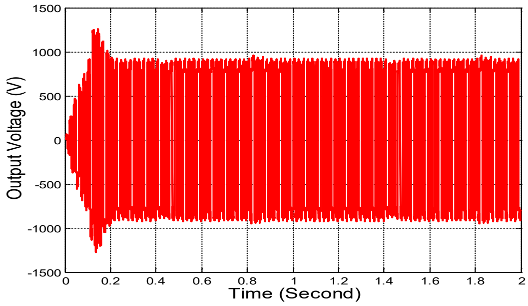


Figure 21. Switched capacitor output voltage

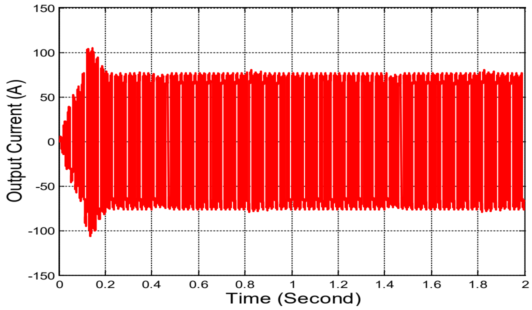


Figure 22. Switched capacitor output current

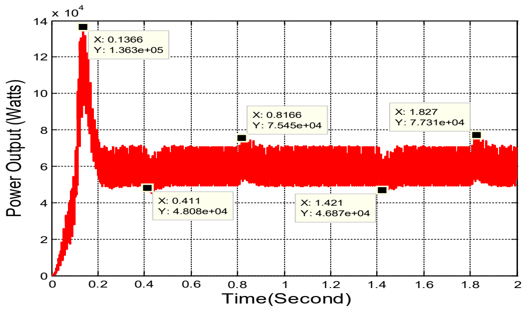


Figure 23. Power Output of the DC-DC boost converter

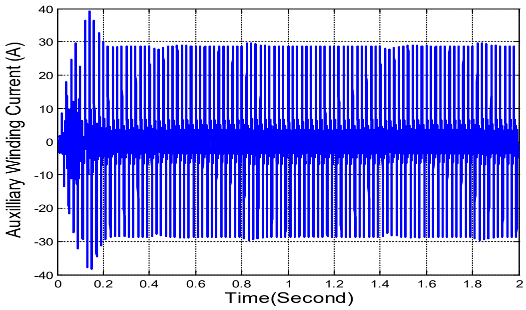


Figure 24. Auxilliary winding current at varied load

The plots for the auxilliary winding and main winding current waveforms are presented in Figures 24 and 25. It shows that much current is drawn by the main winding during machine running operation than the auxilliary winding. In Figures 26 and 27, it is evident that the q-axis rotor current which flows into the the main winding has a greater value in magnitude than the d-axis rotor current connected to the auxilliary winding. The motor speed at varying load is presented in Figure 28. At start and on no-load, the induction motor runs at a very high speed approximately 1639rpm above its synchronous speed value at 0.109 Sec. During a systemic loading at [0.4429 and 0.804] Sec., the motor speed changed periodically from [1497 to 1553] rpm. The speed regulation based on a reference speed value of 1500 rpm and full load speed value of 1497 rpm was obtained as 0.2094.

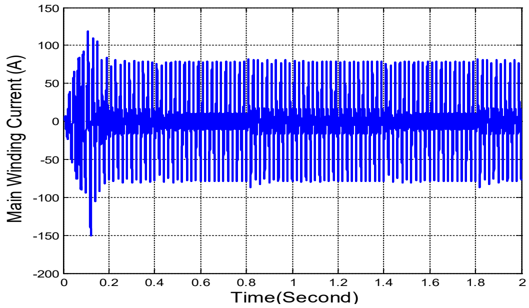


Figure 25. Main winding current at varied load

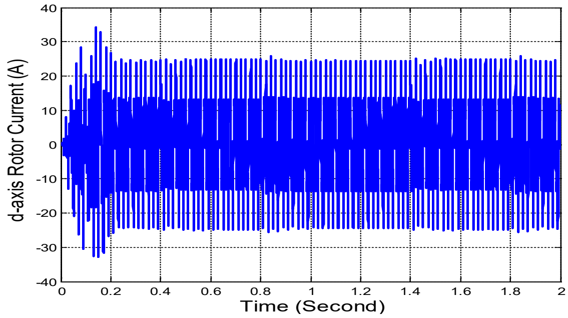


Figure 26. d-axis rotor current at varied load

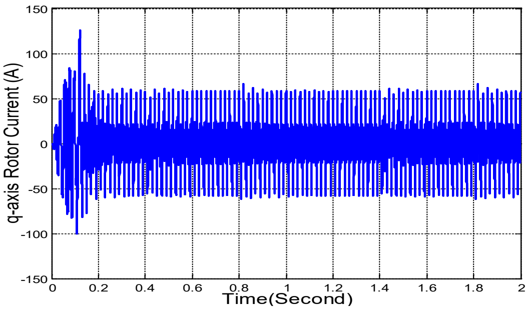


Figure 27. q-axis rotor current at varying load

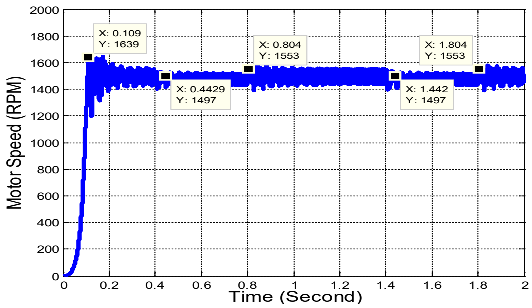


Figure 28. Motor Speed at varying load

The variation in the electromechanical torque value at a varying load condition is shown in Figure 29 while the plot of electromechanical torque against speed is presented in Figure 30. It is evident that the curl at a varying load gradually settled at a full load speed value of 1497 rpm which corresponded to the full load torque value of 22.6 Nm. The applied load torque of the machine is shown in Figure 31 at a varied simulation period of [0.4 to 0.8] Sec. and [1.4 to 1.8] Sec. When the duty cycle was reduced to 0.5, the inductor input current at a varying load reduced correspondingly. The peak value reduced to 167.9A with a reduced rise time of 0.0432 Sec. as shown in Figure 32 which is almost half of the value obtained in Figure 19 at 0.75 duty cycle.

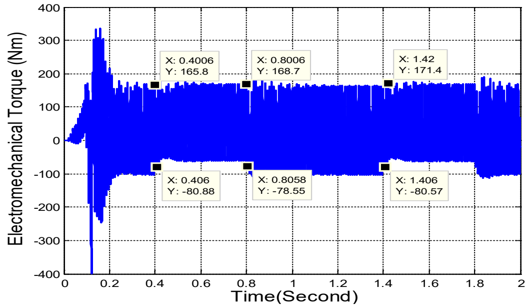

Figure 29. Electromechanical Torque at varying load

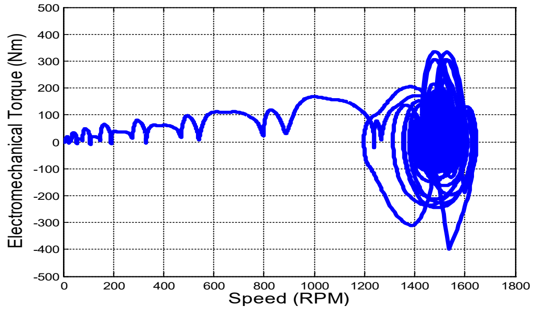

Figure 30. Torque against Speed at varying load

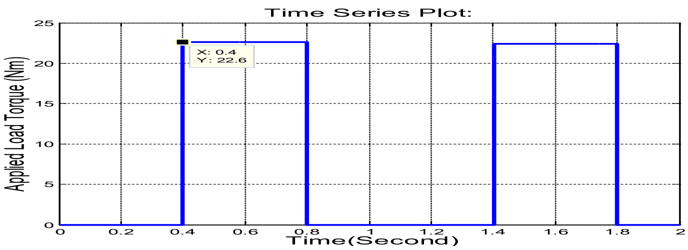

Figure 31. Applied Load Torque

It is also proven that the oscillation rate in Figure 32 is higher than the waveform obtained in Figure 19. The input power at a varying load and 0.5 duty cycle is presented in Figure 33. Although a clear reduction in peak value of 38.81KW and reduced rise time was obtained, there seemed to be a large harmonic oscillation during and after loading. This accounts for the losses and reduced efficiency value. The switched capacitor output voltage and current waveforms at 0.5 duty cycle are shown in Figures 34 and 35. The obvious reduction in their values at a reduced duty cycle is in conformity with equations (5), (6) and (8). The power output of the DC-DC boost converter at 0.5 duty cycle is presented in Figure 36. The variations in the power values as the load changed are depicted in the waveform. An obvious decrease in the output power value was observed which gave rise to a reduced efficiency value of 76.79%.

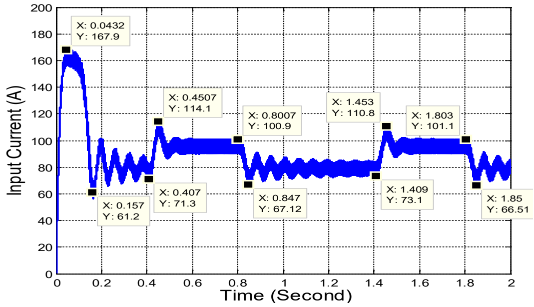

Figure 32. Inductor input Current at a varying load

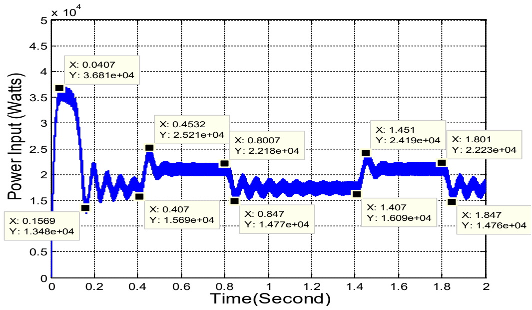

Figure 33. Input Power of the Converter at a varying load

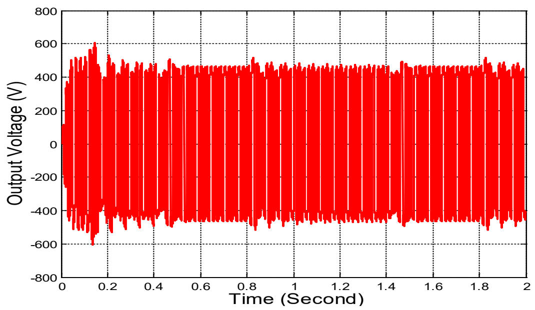

Figure 34. Switched capacitor output voltage

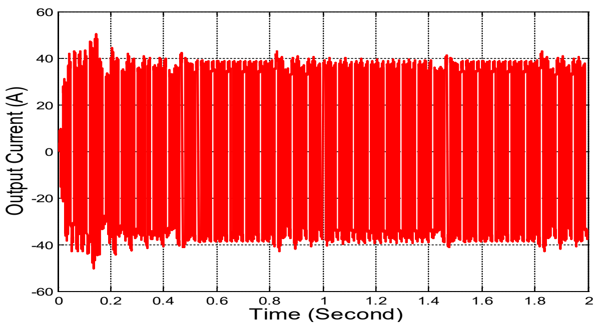

Figure 35. Switched capacitor output current

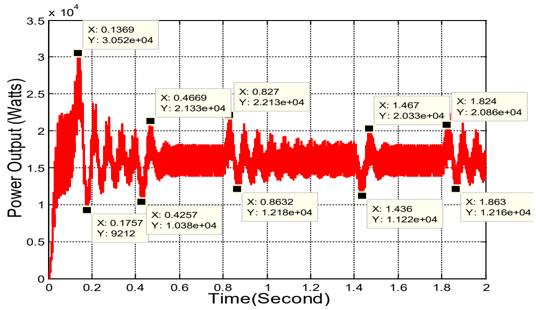


Figure 36. Power Output of the DC-DC boost converter

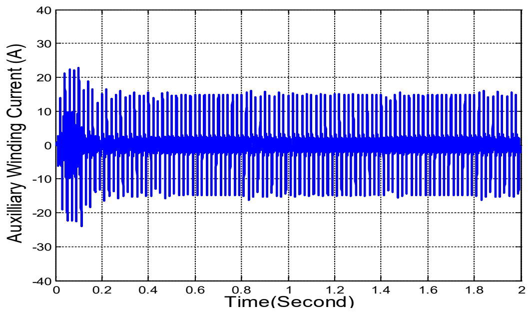


Figure 37. Auxilliary winding current at varied load

The current waveforms for the auxilliary winding and main winding are shown in Figures 37 and 38. It is obvious that more current is drawn by the main winding with a reduced amplitude as compared to Figures 24 and 25 respectively. The waveforms for the dq-axes rotor current at varied load are presented in Figures 39 and 40. A close observation shows that more current is drawn at the q-axis than the d-axis. The speed variation in response to changes in load at 0.5 duty cycle is presented in Figure 41. It is observed that speed value reduced with load variation at reduced duty cycle. Similarly, the changes in the electromechanical torque values at 0.5 duty cycle is shown in Figure 42. It is obvious that more torque ripples are produced at 0.5 duty cycle which accounted for the losses associated with the machine during the drop in voltage. In Figure 43, the plot of torque against speed at varying load is presented at 0.5 duty cycle. A pronounced oscillation was observed before a curl is finally formed at a full load speed value of 1468 rpm. Table 2 shows the comparative performance of the machine at steady state and transient state for 0.5 and 0.75 duty cycle.

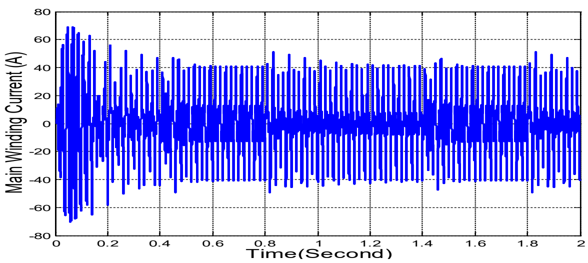


Figure 38. Main winding current at varied load

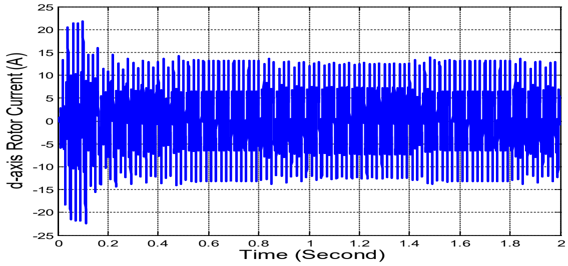


Figure 39. d-axis rotor current at varied load

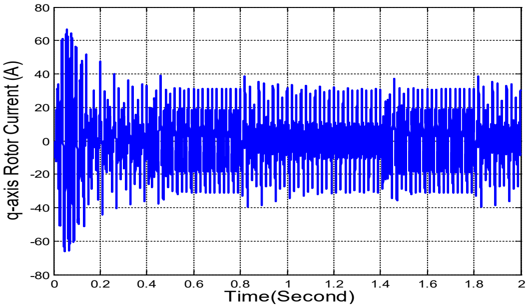


Figure 40. q-axis rotor current at varying load

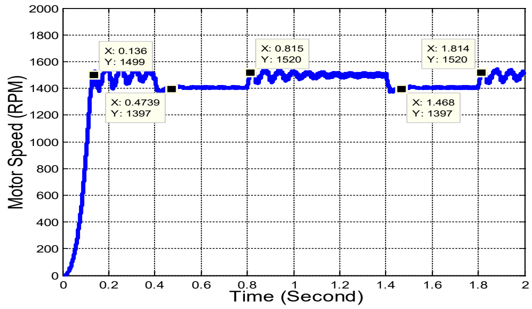


Figure 41. Motor Speed at varying load

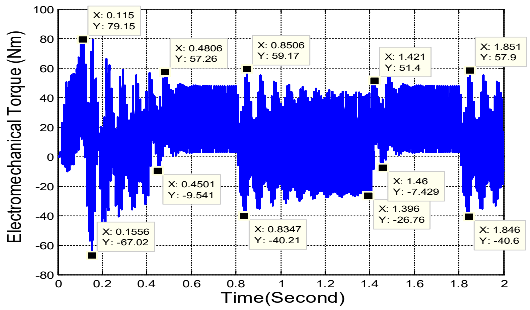


Figure 42. Electromechanical Torque at varying load

Table 2. Machine and Converter performance at steady state and transient state for D = 0.5 and 0.75.

| Parameters | Steady State and Duty Cycle = 0.5 | Transient State and Duty Cycle = 0.5 | Steady State and Duty Cycle = 0.75 | Transient State and Duty Cycle = 0.75 |
|---|---|---|---|---|
| Efficiency (%) | 84.16 | 76.79 | 83.45 | 82.86 |
| Speed Regulation | 0.2255 | 0.2094 | 0.9271 | 0.2086 |

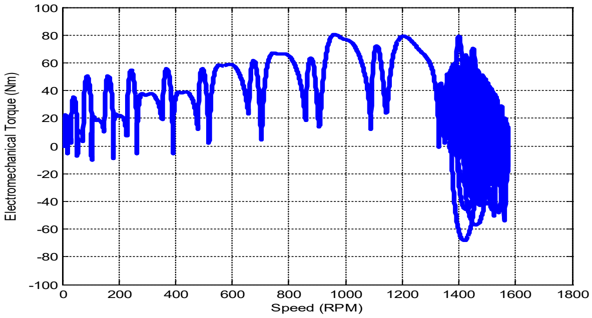

Figure 43. Torque against Speed at varying load

## 5. Conclusion

The torque-speed performance of a single phase capacitor start and capacitor run induction motor (CSCRIM) directly fed by DC-DC-AC boost switched capacitor converter has been compared at different duty cycle values of 0.5 and 0.75 under steady state and dynamic state. It has been established from the simulation results that the single phase induction motor exhibited an excellent dynamic performance at 0.75 duty cycle with high voltage gain, reduced power losses, an enhanced starting torque and an improved efficiency value of 82.86% with a good speed regulation. The simulation results obtained under steady state operation also showed a good percentage reduction in the magnitude of torque pulsations and machine acceleration time at 0.75 converter duty cycle. The increased converter outputs at reduced losses would entail a significant reduction in the running cost of the machine's operation thereby promoting its reliablity in terms of domestic and industrial usage.

## 6. References


[1]. M.S. Dall'Asta, Ivo Barbi, T.B. Lazzarrin. "AC-AC Hybrid Boost Switched Capacitor Converter," *IEEE Trans. Power Electron., Vol.35, no.12, pp.13115-13125, December, 2020.*

[2]. G.V. Silva, J.M. De-Andrade, R.F. Coelho and T.B. Lazzarin. "Switched Capacitor differential boost Inverter: Design, modeling and control," *IEEE Trans. Ind. Electron,. Vol. 67, no.7. pp. 5421-54331, 2020.*

[3]. T.B. Lazzarrin, M.P. Mocceli and I. Barbi. "Split-Phase Switched Capacitor AC-AC Converter," *IET Power Electron. Vol.8, no.6, pp. 918-928, 2015.*

[4]. N.C. DalPont, M.D. Vecchia, G. Waltrich,a nd T.B. Lazzarin. "Step-up Inverter Conceived by the Integration between a full bridge Inverter and a Switched Capacitor Converter," *In Proc. IEEE 13th Brazzillian Power Electronics Conf. Ist Southern Power Electron. Conf. Fortuleza, Brazil, 2015, pp.1-6.*

[5]. J. You and C. Hui. "A Novel Switched Capacitor AC-AC Converter with a ratio of ¼," *In Proc. 17th Int. Conf. Elect. Mech. Syst. Hangzhou. China, 2014, pp.3205-3207.*

[6]. W. Do, I. Oota and K. Eguchi. "A Switched Capacitor AC-AC Converter Using Nested Voltage Equalizers," *In Proc. Telecommun. Inf. Technol. Phalet. Thailand, 2017, pp.314-317.*

[7]. L. He, J. Awang, C. Cheng and T. Li. "A bidirectional bridge Modular Switched-Capacitor based power electronic transformer," *IEEE. Trans. Ind. Electron., Vol. 65, no.1, pp.718-726, Jan. 2014.*

[8]. K. Eguchi, F. Asadi, H. Abe, T. Ishibashi, and H. Sasaki. "Development of a Simple direct Switched Capacitor AC-AC Converter Using Cascade Connection," *Int. J. Innov. Comput. Inf. Control. Vol. 14, pp. 2335-2342, Dec. 2018.*

[9]. T.B. Lazzarin, R.L. Andersena and I. Barbi. "A Switched capacitor Three Phase AC-AC Converter," *IEEE Trans. Ind. Electron. Vol. 62., no. 2, pp. 735-745, Feb. 2015.*

[10]. R.L da Silva, T.B. Lazzarin and I. Barbi. "Reduced Switch Count Step-up/Step down Swicthed Capacitor Three Phase AC-AC Converter," *IEEE Trans. Ind. Electron. Vol.65, no.11, pp. 8422-8432, Nov. 2018.*
[11]. Y. Mu, X. Yang, Y. Xue, Z. Lin, T.Q. Zheng and S. Igarashi. "A bidirectional Switched-Capacitor based AC-AC resonant Converter," *In Proc. IEEE 11th Conf. Ind. Electron. Appl. Hefei, China, 2016, pp.973-977.*
[12]. L. He, T. Zeng and J. Zhang. "The regulatiom Characteristics of Bridge Modular Switched Capacitor AC-AC Converter," *IEEE Access, Vol.7, pp. 147683-147693, 2019.*
[13]. M.Y. Forouzesh, S.A. Stwakoti, A. Gorji and F. Blaabjerg. "Step-up DC-DC Converters: A Comprehensive Review of Voltage Boosting Techniques, Topologies and Applications," *IEEE Trans. Power Electron., Vol. 32, Issue 12, pp. 9143-9178, 2017.*
[14]. J.D. Hardiantoro, "Analysis of Changing of Run capacitor Motor to Start-Run Capacitor Motor," *Journal of Basic and Applied Scientific Research. Vol. 9, no.4, pp. 1-15, 2019.*
[15]. A.I. Mohid and S. Gurneat, "A Review on Influence of Rotor Geometry on the Performance of Single-Phase Capacitor Run Induction Motor," *International Journal of Advanced Research in Electrical/Electronic and Instrumentation Engineering. Vol. 3, no. 6, pp. 10216-10224, 2014.*
[16]. E.I. Idoko, E.S. Obe, J.U. Agber. "Operation of Single Phase Induction Motor with two Identical Stator Windings," *American Journal of Engineering Research. Vol. 5, Issue 6, pp. 13-19, 2016.*
[17]. R. Darbali-Zamora, D.A. Merced-Cirino, A.J. Diaz-Castillo and E.I. Ortiz-Rivera. "Single Phase Induction Motor alternate Start up and Speed Control Method for Renewable eneergy application," *In: International Conf. Renewable Energy Research and Application (ICRERA) Milwauker: IEEE 2014, pp. 743-748.*
[18]. H. Hanafy. "Dynamic Analysis of a New Connection for Dual Voltage operation of Single Phase Capacitor Run Motor," *Journal of Electrical Engineering. Vol. 13, Issue 1. Pp. 1-8, 2013.*
[19]. A. Leicht and K. Makowski. "Analysis of Single-Phase Capacitor Induction Motor Operating at Two Power Line Frequencies," *Archives of Electrical Engineering, Vol. 61, Issue 2, pp. 251-266, 2012.*
[20]. M.S. Jannati, S. Anbaran, S. Asgari, W. Gohi and N. Idris. "A Review on Variable Speed Control Techniques for Efficient Control of Single Phase Induction Motors: Evolution, *Classification, Comparison on Renewable and Sustainable Energy Reviews, Vol. 75, Issue 1, pp. 1306-1319, 2017.*
[21]. C.M. Ong, Dynamic Simulation of Electric Machinery Using MATLAB/SIMULINK. Prentice Hall PTR Upper Saddle River, New Jersey, 1998.
[22]. A.E. Fitzgerald, "Electric Machinery" 5th Edition, McGraw-Hill Inc, New York, 1990.
[23]. J.F. Mora, Electrical Machines. McGraw Hill, New York, 2003.
[24]. P. Krause, O. Wasynczuk, and S.D. Sudhoff, "Analysis of Electric Machinery," McGraw-Hill Inc, 1986.
[25]. M.C. Richard, Electric Drives and Their Control. Oxford University Press: New York, 1995.
[26]. L. Daniel and T.K Philip Control of Induction Machine Drives. CRC press LLC, Illinois, 2002.
[27]. V. Ostovic, Computer-Aided Analysis of Electric Machines prentice Hall International (U.K) Ltd, 1994.

APPENDIX 1

An abridged Simulink model of DC-DC-AC Boost Converter Fed Induction Motor subsystem

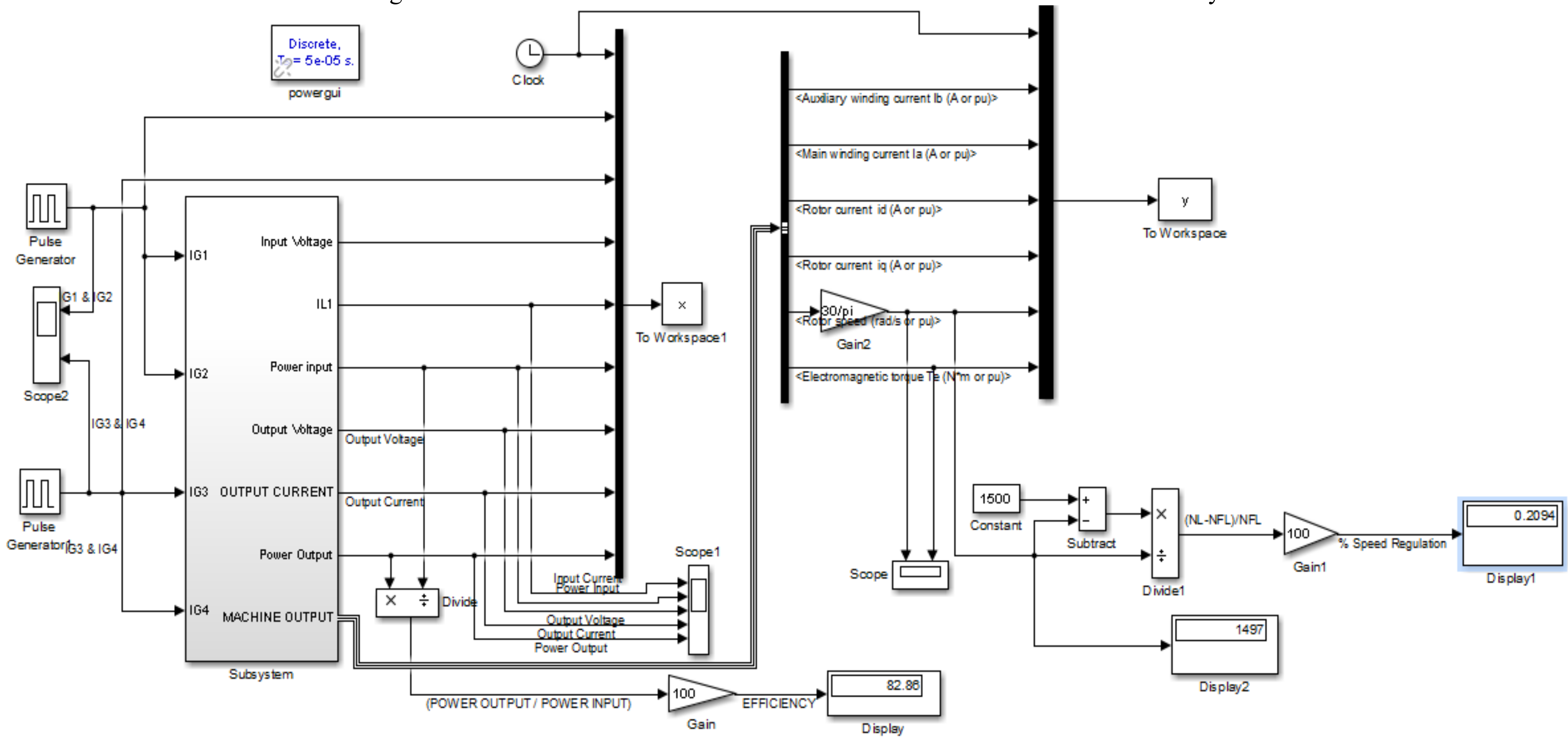

An complete model of DC-DC-AC Boost Converter Fed Induction Motor

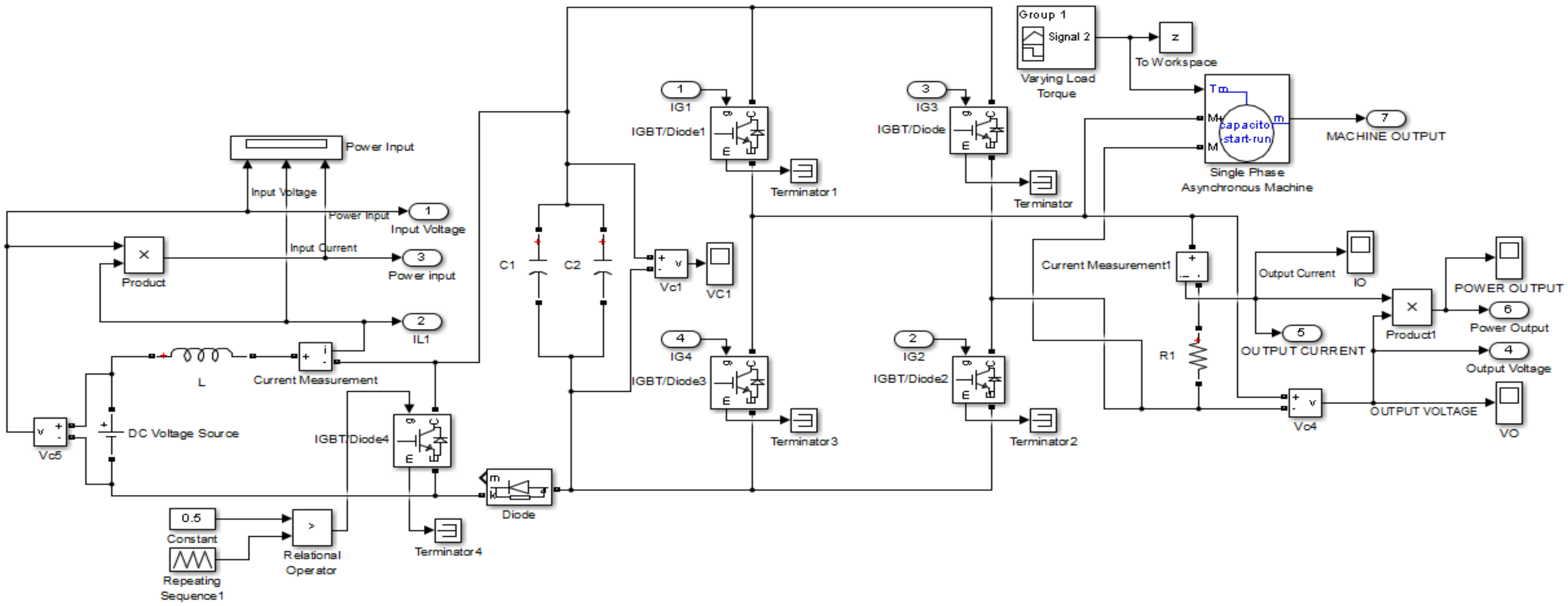


**Crescent Onyebuchi Omeje** received his Bachelor's degree in Electrical Engineering, in 2004 from University of Nigeria, Nsukka. He also obtained his Masters of Engineering (M.Eng) and Doctor of Philosophy (Ph.D) with distinction in 2011 and 2019 respectively in Electrical Engineering, from the same University. He is a Member of Nigeria Society of Engineers (MNSE), a registered member Council for the regulation of Engineering in Nigeria (COREN), a member of the Institute of Electrical/Electronic Engineering (IEEE) and a full-time lecturer in the Department of Electrical/Electronic Engineering, University of Port Harcourt, Rivers State, Nigeria. His research interests are on power electronics, new Energy conversion systems, multilevel inverter applications, smart grid intelligent systems, and Electric Motor drives. email:crescent.omeje@uniport.edu.ng.